

Measurement of the Nonlinear Conducting States of α -(BEDT-TTF)₂I₃ Using Electronic Raman Scattering

Atsuya Ito,¹ Yuto Nakamura,¹ Arao Nakamura,¹ and Hideo Kishida^{1,2,*}

¹*Department of Applied Physics, Nagoya University, Furo-cho, Chikusa-ku, Nagoya 464-8603, Japan*

²*CREST, Japan Science and Technology Agency (JST), Tokyo 102-0076, Japan*

(Received 29 December 2011; revised manuscript received 22 April 2013; published 4 November 2013)

Nonlinear conducting states in a strongly correlated organic electronic system α -(BEDT-TTF)₂I₃ [BEDT-TTF = bis(ethylenedithio)-tetrathiafulvalene] are studied by Raman spectroscopy. Wide-range Raman spectra of nonlinear conducting states provide direct information about conducting properties through the electronic Raman process. A comparison between the behaviors of the electronic modes of BEDT-TTF layers and the vibrational mode of I₃ molecules reveals the formation of nonequilibrium states in which only the electronic parts show the change of states. We obtained a spatial map of the conducting regions of the nonlinear conducting states by utilizing the electronic Raman intensity as a measure of the highly conducting states. A spatially inhomogeneous formation of nonlinear conducting states was observed.

DOI: [10.1103/PhysRevLett.111.197801](https://doi.org/10.1103/PhysRevLett.111.197801)

PACS numbers: 78.30.Jw, 72.20.Ht

Phase control by an external field or stimulus in strongly correlated electron materials such as organic conductors and 3d transition metal materials is one of the challenging issues in solid-state physics [1–3]. To achieve phase control, the field-induced phase needs to be clearly understood. The elucidation of these electronic states and the formation mechanism for these external-field-induced phases is a first step toward field-induced phase control. Nonlinear conducting behaviors, defined as field-induced changes of resistivity, are intriguing phenomena, which are often observed in strongly correlated inorganic and organic electron systems such as Sr₂CuO₃ [4], θ -type bis(ethylenedithio)-tetrathiafulvalene (BEDT-TTF) salts [5,6], potassium-tetracyanoquinodimethane [7,8], and one-dimensional halogen-bridged nickel compounds [9]. However, the electronic state and the mechanisms of domain formation in nonlinear conducting states are controversial.

Among strongly correlated organic materials [3], α -(BEDT-TTF)₂I₃ is one of the most thoroughly investigated compounds. It has been recently discussed from the viewpoints of Dirac electrons [10,11] as well as its unique phase-transition and dielectric properties [12–15]. α -(BEDT-TTF)₂I₃ undergoes a metal-insulator transition at $T_c = 135$ K [16]. Below T_c , charge-rich (valence 0.73 to 0.82) and charge-poor (valence 0.26 to 0.29) sites are arranged alternately along the molecular stacking axis (a axis). Along the b axis, charge-rich and charge-poor molecules are aligned separately [17], leading to striped-pattern charge ordering (CO) [17,18]. The application of an electric field breaks the insulating states, thus lowering the resistivity [14]. Considering that the insulating mechanism is due to the electron correlation effects, we can expect that the origin of the electric-field-induced change is also electronic. However, the detailed electronic states in nonlinear conducting states are unclear.

In this Letter, we describe the nonlinear conducting states in α -(BEDT-TTF)₂I₃ that are revealed by electronic Raman scattering. First, we discuss the electronic Raman spectra of α -(BEDT-TTF)₂I₃ recorded in the absence of an external field. The electronic Raman spectra reveal not only the conducting properties but also the coupling between the electronic and lattice excitations. Then, we discuss the field-induced change in the Raman spectra. The electronic states in the BEDT-TTF layers under an electric field are highly similar to those in the metallic phase, while the state of an insulating I₃ layer is different from that in the metallic phase. This is a strong indication of the fact that the observed nonlinear conducting state is a nonequilibrium state resulting from the breakdown of the insulating mechanism, namely, charge ordering. Moreover, we could identify the spatial features in the formation of the nonlinear conducting states from mapping measurements of the microscopic electronic Raman spectra. In this way, we clarified the electronic states and formation mechanism of nonlinear conducting states in α -(BEDT-TTF)₂I₃.

We synthesized α -(BEDT-TTF)₂I₃ crystals by the electrochemical method [19]. The absorption spectrum was measured for a thin crystal having 2.8 μm thickness. Raman and electrical conductivity measurements were performed using samples that were typically 10 μm thick. In the Raman measurements, a He-Ne excitation laser with a wavelength of 632.8 nm was mainly used. The sensitivity of the optical system was corrected using a standard light source. In the nonlinear conduction experiments, carbon paste was used for the electrodes.

Figure 1(a) shows an absorption spectrum at 73 K with polarization along the a axis. The spectrum has a broad structure around 2000 cm^{-1} and a dip around 1500 cm^{-1} . The broad structure was assigned to the charge transfer transition along the stacking column [20–23].

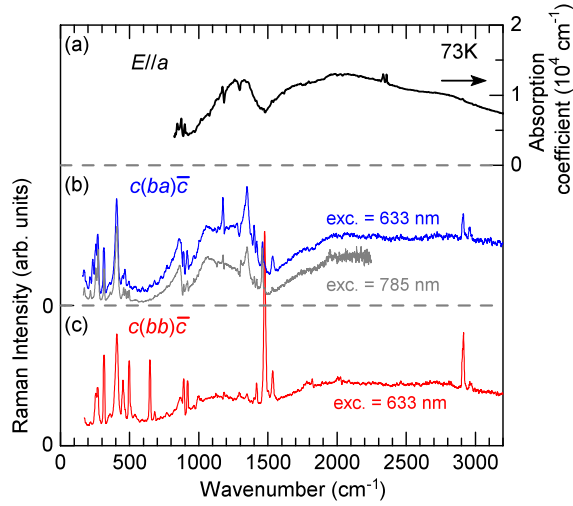


FIG. 1 (color online). Absorption (a) and Raman scattering spectra [(b) and (c)] of α -(BEDT-TTF) $_2$ I $_3$ crystal measured at 73 K. In the representation of configurations such as $c(ba)\bar{c}$, the first and fourth characters indicate the traveling directions of the incident and scattered light, respectively. The second and third characters are the polarizations of the incident and scattered light, respectively.

Figures 1(b) and 1(c) show the Raman spectra of the configurations $c(ba)\bar{c}$ and $c(bb)\bar{c}$. Because the Raman spectra measured with two different excitation wavelengths are similar, we can judge that broad background structure as well as the sharp peaks are Raman signals. A dip around 1500 cm^{-1} is also common in the absorption and Raman spectra, and it has a half-width of about 200 cm^{-1} . The depth of the dip in $c(ba)\bar{c}$ is larger than that in $c(bb)\bar{c}$, but the vibrational peak at 1476 cm^{-1} [24] is larger for $c(bb)\bar{c}$. Notably, the broad structure in $c(ba)\bar{c}$ resembles that in the absorption spectrum. Therefore, it is attributed to the charge transfer transition, similar to the assignment of the absorption spectrum [21].

The absorption process is a one-photon transition from the ground state to excited states. However, in the Raman process, two photons, i.e., two optical transitions, are involved, where one photon is related to the excitation to the intermediate state and the other photon is emitted as a Raman signal [25]. Generally, processes involving two optical transitions, such as Raman scattering, have access to excited states with different symmetries than those accessible by absorption processes. Therefore, Raman spectra do not always correspond to absorption spectra. Nonetheless, the observed absorption spectra and Raman spectra were similar. This might indicate that the density of states of the excited states reached by two sequential optical transitions is similar to that of the one-photon excited states. The similarity between Raman spectra and one-photon excitation spectra was discussed for cuprates, for which the coherence of ordered states is an important factor [26,27].

The temperature dependence of the Raman spectra between 10 and 170 K in $c(ba)\bar{c}$ is shown in Fig. 2(a). With increasing temperature, the vibrational structure became blurred and the electronic Raman signals became broadened. In order to highlight the effect of the temperature change, we analyzed the spectral shape using a simplified model. Almost all sharp peaks were symmetric, while three structures, located at 880 , 1180 , and 1500 cm^{-1} , showed characteristic spectral shapes due to significant coupling with the electronic systems. The first two structures had an asymmetric spectral shape at 73 K, as shown in Fig. 1(b). The third structure is a large dip, as mentioned above. The spectral shapes of these three structures are all typical Fano-type structures. In our case, some sharp vibrational modes couple to the broad charge excitation, causing quantum-mechanical interference.

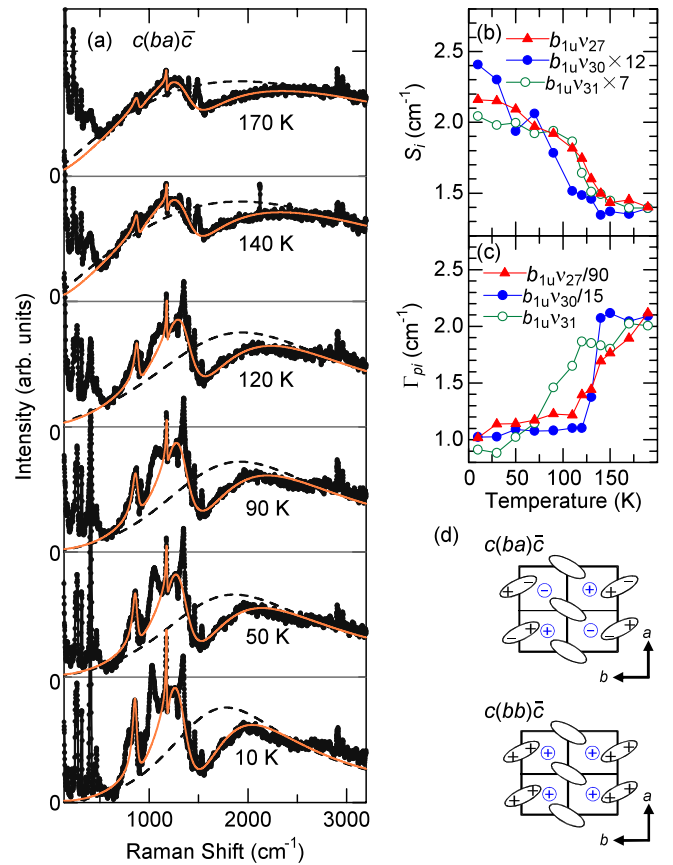


FIG. 2 (color online). (a) Temperature dependence of Raman spectra of α -(BEDT-TTF) $_2$ I $_3$ with an excitation wavelength of 633 nm (dots: experimental, solid line: fitting calculation, dotted lines: the component of electronic excitation in the fitting calculation). (b) Coupling constant S_i between electronic excitation and vibrational modes. (c) Damping factor of the i th vibrational modes. (d) Possible configurations of the symmetries of electronic excitation and vibrational modes in the BEDT-TTF layer for $c(ba)\bar{c}$ and $c(bb)\bar{c}$ polarization configurations. Ellipses indicate BEDT-TTF molecules. The symbols in the circles and the ellipses indicate the phase of electronic excitation and vibration. I $_3$ molecules are omitted.

We adopted the Fano analysis procedure, which was applied to high-temperature superconductors by Chen *et al.* [28]. We modified the model to fit our case by assuming an electronic excitation consisting of one asymmetric Lorentzian and three vibrational modes and used the following formula:

$$I(\omega) = A[n(\omega) + 1]T_e^2 \left\{ \chi_{\text{Im}}(\omega) + \sum_{i=1}^3 \frac{1}{\Gamma_{vi}(1 + \varepsilon_i^2)} \times \left[\frac{Z_i^2}{S_i^2} + 2\chi_{\text{Im}}(\omega)\varepsilon_i Z_i - \chi_{\text{Im}}(\omega)^2 S_i^2 \right] \right\},$$

where $\Gamma_{vi} = \Gamma_{pi} + S_i^2 \chi_{\text{Im}}(\omega)$, $\omega_{vi} = \omega_{pi} + S_i^2 \chi_{\text{Re}}(\omega)$, $Z_i = S_i(T_{pi}/T_e) + S_i^2 \chi_{\text{Re}}(\omega)$, and $\varepsilon_i = (\omega - \omega_{vi})/\Gamma_{vi}$. $I(\omega)$ is the Raman intensity at frequency ω , and $n(\omega)$ is the Bose distribution function. T_e and T_{pi} are the Raman matrix elements of the transition from the ground state to the electronic excited and i th vibrational states, respectively. The real and imaginary parts of the response function of the electronic parts $\chi_e(\omega)$ are $\chi_{\text{Re}}(\omega)$ and $\chi_{\text{Im}}(\omega)$: $\chi_e(\omega) = -\chi_{\text{Re}}(\omega) + i\chi_{\text{Im}}(\omega)$. Γ_{pi} is the damping factor of the i th vibrational mode, and S_i is the coupling constant between the electronic excitation and the i th vibrational mode. In the fitting procedure, we assumed that the electronic excitation was represented by the following modified Lorentzian [29]: $\chi_e(\omega) = (\omega_e^2 - \omega^2 - i\omega\Gamma_e)^{-1}$, $\Gamma_e(\omega, T) = [(\alpha\omega)^2 + (\beta T)^2]^{1/2}$. Here, ω_e and Γ_e are the characteristic frequency and damping frequency of the electronic excitation, respectively, α and β are the width parameter and the asymmetric parameter, respectively, and T is the temperature.

The fitting results reproduce the overall spectral shape and the asymmetric Fano spectral shape as shown in Fig. 2(a). The obtained parameters S_i and Γ_{pi} are shown in Figs. 2(b) and 2(c), respectively. The coupling constants S_i decrease gradually with increasing temperature. This indicates that the charge or valence fluctuates even below T_c . The partial collapse of the charge ordering and the mobile nature of the electrons reduce the coupling between the electronic and vibrational excitations. The fluctuation below T_c is consistent with previous observations using terahertz spectroscopy [30]. The damping factors Γ_{pi} suddenly increase at a temperature slightly below T_c , possibly due to valence dispersion above T_c resulting from competition between various phases [31,32].

The Fano-like features of the 880, 1180, and 1500 cm^{-1} vibrational structures were more clearly observed in $c(ba)\bar{c}$ than in $c(bb)\bar{c}$. This can be explained by assigning the origin of these structures not to the molecular a_g mode, but to b_{1u} or b_{2u} modes. A schematic explanation of the activation mechanism of the molecular Raman-inactive modes in crystal is shown in Fig. 2(d) [33]. In $c(ba)\bar{c}$, the electronic excitation in the first quadrant (upper-right area of the unit cell) and the third quadrant have the same symmetry between the ground state and the excited state.

The second (upper left) and fourth quadrants have the opposite symmetry. As for the molecular vibration, the b_{1u} modes are represented by positive and negative signs within ellipses in Fig. 2(d). When the symmetry of the excitation and the vibration match, interference can occur. Figure 2(d) shows that the electronic excitation can be connected with the molecular b_{1u} excitation in $c(ba)\bar{c}$. We assign the 880, 1180, and 1500 cm^{-1} structures to the $b_{1u}\nu_{31}$, $b_{1u}\nu_{30}$, and $b_{1u}\nu_{27}$ modes of BEDT-TTF molecules, respectively, [34].

The current-induced change in the Raman spectra in $c(bb)\bar{c}$ measured at 73 K is shown in Fig. 3(a). With

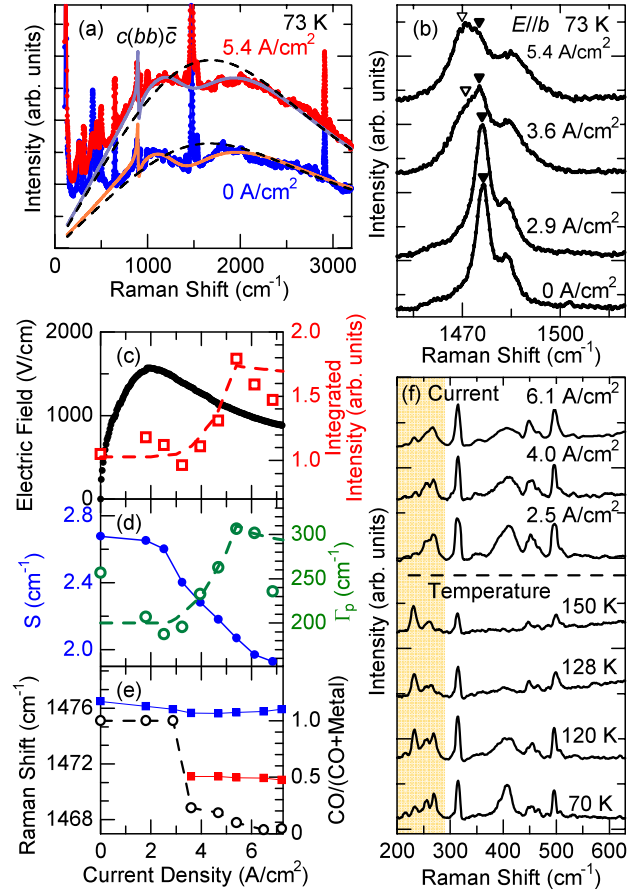


FIG. 3 (color online). (a) Current dependence of the Raman spectra. Dots represent the experimental results, and solid lines show the fitting calculation. Dotted lines show the component of electronic excitation in the fitting calculations. (b) Current dependence of the $a_g\nu_3$ mode. Filled triangles: CO mode, open triangles: metallic. (c) Current dependence of the electric field (filled circles) and integrated intensity (open squares with an added visual guide) of the $a_g\nu_3$ modes. (d) Current dependence of the coupling constant S (filled) and damping factor of the vibrational mode Γ_p (open). (e) Current dependence of the Raman peak wavenumber (solid). The ratio of the CO component is also shown (open). (f) Current and temperature dependence of the $c(bb)\bar{c}$ Raman spectra. Current dependence was measured at 71 K. All the Raman spectra shown in this figure were measured with an excitation of 633 nm.

increasing current density, the integrated intensity of the Raman spectra increases drastically and the $a_g\nu_3$ mode around 1480 cm^{-1} shows a conspicuous spectral change, as shown in Fig. 3(b). It has been established that the $a_g\nu_3$ mode can be used as a measure of the electronic states [24]. In our case, the 1476 cm^{-1} mode [filled inverted triangles in Fig. 3(b)] indicates the CO states, while the 1471 cm^{-1} mode (open inverted triangle) indicates the metallic states. Figure 3(b) shows that the metallic state is formed above 3.6 A/cm^2 and that the CO and metallic states coexist.

The conduction characteristics of this sample are shown in Fig. 3(c). Above 2.0 A/cm^2 , the electric field between the electrodes drops, corresponding to negative differential resistance (NDR). In the NDR region, the integrated intensity of the Raman signal increases. The dip structure centered around 1500 cm^{-1} can be reproduced by a similar Fano analysis of the $c(ba)\bar{c}$ spectra, as shown in Fig. 3(a). The obtained parameters are shown in Fig. 3(d). With increasing current density, the coupling constant S between the electronic components and the $a_g\nu_3$ mode decreases and the damping factor Γ_p of the $a_g\nu_3$ mode increases. Thus, current injection leads to a decrease in the coupling between the vibrational modes and electronic excitations due to the enhancement of the mobile nature of electrons. The results of a Lorentzian analysis of the $a_g\nu_3$ modes are plotted in Fig. 3(e). Above 3.6 A/cm^2 , the 1471 cm^{-1} metallic peak can be discerned. The CO mode and the metallic mode show only a slight shift. However, the weight of the CO mode continuously decreases above 3.6 A/cm^2 and almost disappears at around 7 A/cm^2 . Thus, the transition from CO to the metallic states develops continuously in the NDR regions.

Figure 3(f) shows the current and temperature dependence of the $c(bb)\bar{c}$ Raman spectra. A notable difference was observed between the two dependences below 290 cm^{-1} . The 232-cm^{-1} mode is assigned to the two-vibrational mode of I_3 stretching ($I_3 a_g\nu_1$) [35], which do not play significant roles for the electronic states. As the temperature increases, this mode is significantly enhanced, but it is not enhanced when the current density is increased. Namely, the lattice state of the current-induced state does not correspond to the high temperature state, although the other Raman peaks, such as the BEDT-TTF mode around 400 cm^{-1} in the conducting layer, have current dependences that are similar to their temperature dependences. Specifically, considering that the behaviors of Raman signals of the insulating (I_3) and the conducting (BEDT-TTF) layers are different, the revealed state can be regarded as a nonequilibrium state in which only the electronic state becomes metallic and similar to the high-temperature phase, and the lattice state remains in the low-temperature phase.

Thus, the electronic Raman intensity is a good measure of conduction characteristics. We performed mapping measurements of $c(bb)\bar{c}$ Raman spectra, integrating the Raman intensity between 1220 and 1700 cm^{-1} .

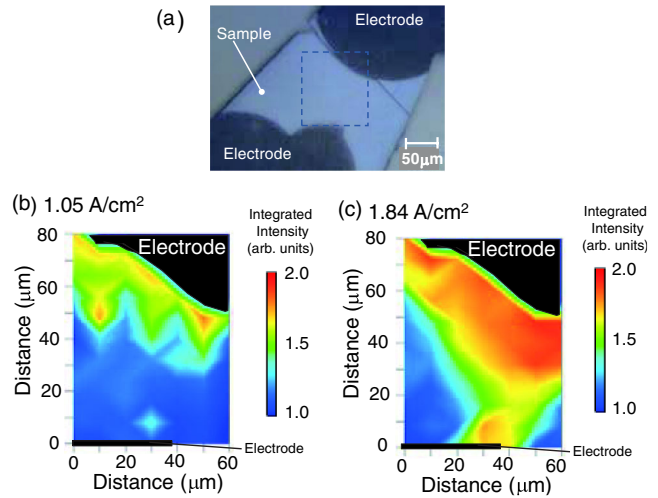


FIG. 4 (color online). (a) Experimental configuration for the mapping measurements. Dotted line indicates the measured area. Map of Raman intensity (73 K) integrated between 1220 and 1700 cm^{-1} measured at two current densities, (b) 1.05 and (c) 1.84 A/cm^2 . See also the Supplemental Material [36].

The configuration of the electrodes and sample is shown in Fig. 4(a). The results of the mapping measurements at two current densities in the NDR region for this sample are shown in Figs. 4(b) and 4(c). At a lower current density, the integrated intensity increases only in certain locations, and this higher Raman intensity indicates the conducting areas. At higher current density, the higher intensity region expands, and the two electrodes are connected by a conducting region on the crystal surface. Even in the high-current condition, there are areas in which the Raman intensity shows little change. Thus, we conclude that the nonlinear conducting current path in $\alpha\text{-(BEDT-TTF)}_2I_3$ is neither spatially homogeneous nor filamentary, but has a domain structure that is $20\text{--}30\text{ }\mu\text{m}$ wide. Considering that such domain structures are macroscopic, a cooperative mechanism induced by the injected current might work.

In summary, nonlinear conducting states in $\alpha\text{-(BEDT-TTF)}_2I_3$ were studied by the electronic Raman method. The electronic Raman spectra reflect the charge excitation and can be characterized by the Fano interference between the electronic excitation and lattice modes. The Raman spectra of the nonlinear conducting states indicate that the electronic parts are similar to the high-temperature metallic phase. However, the vibrational modes of I_3 molecules indicate that the temperature of the crystals is not significantly increased. Specifically, the nonlinear conducting states are achieved by the electronic change of the state in the two-dimensional conducting layer consisting of BEDT-TTF molecules. Moreover, using the intensity of the electronic Raman signals as a probe of the conducting properties, we clarified the spatial distribution of their highly conducting states. The nonlinear conducting path is not spatially homogeneous, and conducting domains are formed that are a few tens of microns in size.

We thank H. Sawa and E. Nishibori for the x-ray evaluation of the crystals, and S. Iwai and K. Iwano for valuable discussions. This study was supported in part by KAKENHI (No. 23225005) from the Japan Society for the Promotion of Science.

*kishida@nuap.nagoya-u.ac.jp

- [1] E. Dagotto, *Science* **309**, 257 (2005).
- [2] *The 3rd International Conference on Photo-Induced Phase Transitions and Cooperative Phenomena (PIPT3)*, J. Phys: Conf. Series Vol. 148, edited by K. Tanaka, T. Ogawa, H. Hashimoto, and S. Koshihara (IOP, Bristol, 2009).
- [3] G. Saito and Y. Yoshida, *Bull. Chem. Soc. Jpn.* **80**, 1 (2007).
- [4] Y. Taguchi, T. Matsumoto, and Y. Tokura, *Phys. Rev. B* **62**, 7015 (2000).
- [5] F. Sawano, I. Terasaki, H. Mori, T. Mori, M. Watanabe, N. Ikeda, Y. Nogami, and Y. Noda, *Nature (London)* **437**, 522 (2005).
- [6] Y. Takahide, T. Konoike, K. Enomoto, M. Nishimura, T. Terashima, S. Uji, and H. M. Yamamoto, *Phys. Rev. Lett.* **98**, 116602 (2007).
- [7] R. Kumai, Y. Okimoto, and Y. Tokura, *Science* **284**, 1645 (1999).
- [8] H. Kishida, T. Ito, A. Ito, and A. Nakamura, *Appl. Phys. Express* **4**, 031601 (2011).
- [9] H. Kishida, T. Ito, A. Nakamura, S. Takaishi, and M. Yamashita, *J. Appl. Phys.* **106**, 016106 (2009).
- [10] S. Katayama, A. Kobayashi, and Y. Suzumura, *J. Phys. Soc. Jpn.* **75**, 054705 (2006).
- [11] N. Tajima, S. Sugawara, R. Kato, Y. Nishio, and K. Kajita, *Phys. Rev. Lett.* **102**, 176403 (2009).
- [12] S. Iwai, K. Yamamoto, A. Kashiwazaki, F. Hiramatsu, H. Nakaya, Y. Kawakami, K. Yakushi, H. Okamoto, H. Mori, and Y. Nishio, *Phys. Rev. Lett.* **98**, 097402 (2007).
- [13] Y. Kawakami, T. Fukatsu, Y. Sakurai, H. Unno, H. Itoh, S. Iwai, T. Sasaki, K. Yamamoto, K. Yakushi, and K. Yonemitsu, *Phys. Rev. Lett.* **105**, 246402 (2010).
- [14] K. Tamura, T. Ozawa, Y. Bando, T. Kawamoto, and T. Mori, *J. Appl. Phys.* **107**, 103716 (2010).
- [15] T. Ivek, B. Korin-Hamzić, O. Milat, S. Tomić, C. Clauss, N. Drichko, D. Schweitzer, and M. Dressel, *Phys. Rev. Lett.* **104**, 206406 (2010).
- [16] K. Bender, I. Hennig, D. Schweitzer, K. Dietz, H. Endres, and H. J. Keller, *Mol. Cryst. Liq. Cryst.* **108**, 359 (1984).
- [17] T. Kakiuchi, Y. Wakabayashi, H. Sawa, T. Takahashi, and T. Nakamura, *J. Phys. Soc. Jpn.* **76**, 113702 (2007).
- [18] H. Seo, *J. Phys. Soc. Jpn.* **69**, 805 (2000).
- [19] H. Anzai, M. Tokumoto, T. Ishiguro, G. Saito, H. Kobayashi, R. Kato, and A. Kobayashi, *Synth. Met.* **19**, 611 (1987).
- [20] M. G. Kaplunov, E. B. Yagubskii, L. P. Rosenberg, and Y. G. Borodko, *Phys. Status Solidi A* **89**, 509 (1985).
- [21] M. Meneghetti, R. Bozio, and C. Pecile, *Synth. Met.* **19**, 143 (1987).
- [22] C. Clauss, N. Drichko, D. Schweitzer, and M. Dressel, *Physica (Amsterdam)* **405B**, S144 (2010).
- [23] M. Dressel and N. Drichko, *Chem. Rev.* **104**, 5689 (2004).
- [24] R. Wojciechowski, K. Yamamoto, K. Yakushi, M. Inokuchi, and A. Kawamoto, *Phys. Rev. B* **67**, 224105 (2003).
- [25] R. Loudon, *The Quantum Theory of Light* (Oxford University Press, New York, 2000), p. 372.
- [26] F. Venturini, Q.-M. Zhang, R. Hackl, A. Lucarelli, S. Lupi, M. Ortolani, P. Calvani, N. Kikugawa, and T. Fujita, *Phys. Rev. B* **66**, 060502(R) (2002).
- [27] T. P. Devereaux and R. Hackl, *Rev. Mod. Phys.* **79**, 175 (2007).
- [28] X. K. Chen, E. Altendorf, J. C. Irwin, R. Liang, and W. N. Hardy, *Phys. Rev. B* **48**, 10530 (1993).
- [29] F. Slakey, M. V. Klein, J. P. Rice, and D. M. Ginsberg, *Phys. Rev. B* **43**, 3764 (1991).
- [30] H. Nakaya, K. Itoh, Y. Takahashi, H. Itoh, S. Iwai, S. Saito, K. Yamamoto, and K. Yakushi, *Phys. Rev. B* **81**, 155111 (2010).
- [31] Y. Yue, K. Yamamoto, M. Uruichi, C. Nakano, K. Yakushi, S. Yamada, T. Hiejima, and A. Kawamoto, *Phys. Rev. B* **82**, 075134 (2010).
- [32] Y. Tanaka and K. Yonemitsu, *J. Phys. Soc. Jpn.* **77**, 034708 (2008).
- [33] If we approximate the symmetry of the unit cell including four independent BEDT-TTF molecules by C_{2h} , the four molecular b_{1u} modes are found to be one Raman-active A_g and three infrared-active B_u modes in the crystal. The A_g mode can be observed in both parallel- and cross-polarization configurations.
- [34] M. E. Kozlov, K. I. Pokhodnia, and A. A. Yurchenko, *Spectrochim. Acta, Part A* **43**, 323 (1987).
- [35] R. Świetlik, D. Schweitzer, and H. J. Keller, *Phys. Rev. B* **36**, 6881 (1987).
- [36] See Supplemental Material <http://link.aps.org/supplemental/10.1103/PhysRevLett.111.197801> for additional mapping results.